ADVANCED MATERIALS INTERFACES
www.advmatinterfaces.de

Ternary $FePSe_3$ Atomic Layers with Competitive Temperature Coefficient of Resistance for Uncooled Infrared Bolometers

Alei Li, Yanfeng Ge, Yuan Gan, Yulu L. Ren, Yingjie He, Qianxue Chen, Peipei Wang, Kai Zhang, Shengyuan A. Yang, Judy Z. Wu, Rui Chen, Liyuan Zhang,* and Youpin Gong**

The semiconducting metal phosphorus trichalcogenides (MPX_3, X = S, Se), a new family of layered atomic materials similar to the transition-metal dichalcogenides, have recently attracted great attention owing to their 2D magnetic properties as well as their wide range of tunable bandgaps, which can lead to promising applications in spintronic and optoelectronic devices. Herein, an uncooled bolometer based on $FePSe_3$ atomic layers is reported, on which a competitive temperature coefficient of resistance (TCR) of ≈–2.96% K^{-1} at room temperature is observed. In detecting infrared radiation (980–1550 nm) at room temperature using the $FePSe_3$ bolometer, high responsivity exceeding 10^8 V W^{-1} and specific detectivity up to 10^9 Jones are achieved, which can be attributed to the combined advantages of the competitive room-temperature TCR and natural thermal isolation between the inner layers of $FePSe_3$ and the environment. This result reveals a remarkable property of $FePSe_3$ atomic layers and paves the way toward new types of bolometers with high sensitivities.

1. Introduction

Bolometers have been widely adopted for detecting infrared (IR) radiation for a variety of applications including thermal imaging, astronomy, health care, and security. A key advantage of the bolometers is that they can work at room temperature without cooling,[1–7] which has been a major limitation for cooled photodetectors based on low bandgap semiconductors such as HgCdTe,[8–11] II–VI and III–V semiconducting superlattices,[12–17] and quantum wells,[18–24] to reduce the dark current and enhance the signal-to-noise ratio. As bolometers measure the resistance change (ΔR) caused by temperature variation (ΔT) under the infrared illumination, high temperature coefficient of

A. L. Li
School of Physics
Harbin Institute of Technology
Harbin 150001, China

A. L. Li, Y. Gan, Q. X. Chen, P. P. Wang, L. Y. Zhang
Department of Physics
Southern University of Science and Technology
Shenzhen 518055, China
E-mail: zhangly@sustech.edu.cn

Y. F. Ge, Y. L. Ren
State Key Laboratory of Metastable Materials Science and Technology and Key Laboratory for Microstructural Material Physics of Hebei Province
School of Science
Yanshan University
Qinhuangdao 066004, China

Y. J. He, Y. P. Gong
College of Physics
Center for Quantum Materials and Devices
at Institute of Advanced Interdisciplinary Studies
Soft Matter and Interdisciplinary Research Center
Chongqing University
Chongqing 400044, China
E-mail: gongyp@cqu.edu.cn

K. Zhang
School of Science and Engineering
The Chinese University of Hong Kong, Shenzhen
Shenzhen 518172, China

S. A. Yang
Research Laboratory for Quantum Materials
Singapore University of Technology and Design
Singapore 487372, Singapore

J. Z. Wu
Department of Physics and Astronomy
University of Kansas
Lawrence, KS 66045, USA

R. Chen
Department of Electrical and Electronic Engineering
Southern University of Science and Technology
Shenzhen 518055, China
E-mail: chenr@sustech.edu.cn

The ORCID identification number(s) for the author(s) of this article can be found under https://doi.org/10.1002/admi.202100491.

DOI: 10.1002/admi.202100491

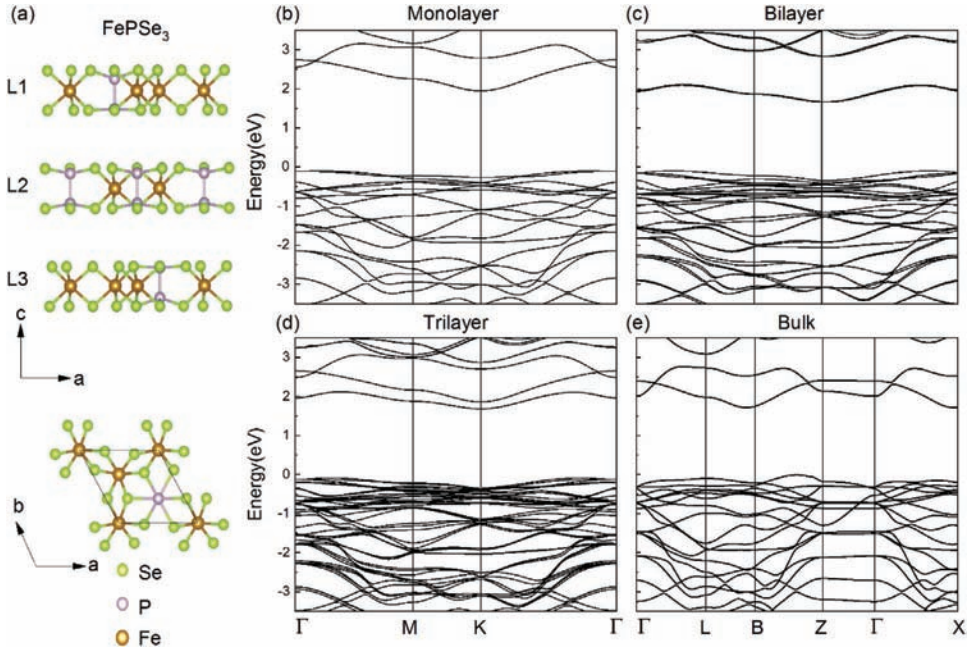

Figure 1. a) Layered structure (side view) of bulk $FePSe_3$ (upper) and in-plane lattice structure (top view) of a monolayer $FePSe_3$ (lower). The electronic band structures of the $FePSe_3$ material with b) monolayer, c) bilayer, d) trilayer, and e) bulk structures.

resistance (TCR) of the bolometer materials is critical. The commercially adopted materials have TCR values typically in the range of a few percent. For example, metallic Ti, Ni, or Pt have TCR 1% K ^{1},[25–28] semiconducting amorphous silicon[6,29,30] and vanadium oxide (VO_x)[28,31,32] have TCR in the range of 2–4 and 2% K ^{1}, respectively. In addition, recently reported polycrystalline ceramic composites with large room-temperature TCR also show a promise for applications.[33,34] Since ΔR TCR ΔT, the bolometer detectivity may be limited under low infrared light intensity[35,36] and/or poor thermal isolation of the bolometer. Therefore, a major challenge in the f eld is to explore new materials which can further improve the detectivity of bolometers and work under uncooled conditions.[3–5,37,38]

The metal phosphorus trichalcogenides (MPX_3, X S, Se) are a family of 2D layered atomic materials, similar to the transition-metal dichalcogenides, with high chemical diversity and wide range of tunable bandgaps where the bandgaps in MPS_3 (M Mn, Fe, Ni, Zn, Cd, and $In_{2/3}$) and $MPSe_3$ (M Mn, Fe, and $In_{2/3}$) range from 1.3 to 3.5 eV.[39–43] Although the optical bandgap of $FePSe_3$ is 1.3 eV, it is worth noting that the Fe^{2} ions are nearly octahedrally coordinated in the $FePSe_3$ crystal and the electronic conf guration of the Fe^{2} is $3d^6(^5D)$ in an octahedral ligand f eld. In a crystal f eld, the ^5D state splits into a $^5T_{2g}$ orbital triplet (ground state) and a ^5E_g orbital doublet (excited state) when Fe^{2} in the high spin state. The $^5T_{2g}$ ^5E_g transition energy in $FePSe_3$ is located near 0.81 eV (1550 nm) at 300 K, which corresponds to an absorption band ranging from 0.75 (1650 nm) to 0.89 eV (1400 nm).[44] This suggests that the $FePSe_3$ could be a promising material for near-infrared (NIR) and short-wave infrared (SWIR) detection. In particular, the conventional semiconductor bolometers must be suspended to reduce their thermal link to the surrounding for high signal-to-noise ratios. In contrast, the $FePSe_3$ atomic-layer stack with the weak van der Waals (vdW) interlayer force inherits a naturally suspended structure that can reduce ef ectively the thermal link to the supporting substrate. Motivated by this, we present the f rst systematic study of the $FePSe_3$ bolometers with thicknesses ranging from 6 layers (6 L) to 74 L using the mechanical exfoliation and dry transfer method. A competitive room-temperature TCR of (2–3)% K ^{1} has been obtained, which is comparable to that for the current state-of-the-art commercial VO_x bolometers. Remarkably, high responsivity (R_v) exceeding 10^8 V W ^{1} and specif c detectivity (D^*) up to 10^9 Jones (1 Jones 1 cm $Hz^{1/2}$ W ^{1}) under 1550 nm light illumination have been obtained on uncooled $FePSe_3$ bolometers, suggesting 2D atomic layer materials are promising candidates for high sensitivity IR detection.

2. Results and Discussion

In the monolayer structure of $FePSe_3$, $(P_2Se_6)^4$ bipyramids are arranged in a triangular lattice and wrapped in a six-Fe ring (**Figure 1**a). The point symmetry group for monolayer structure is D_{3d} when the bulk is in space group R-3 (No. 148). The bulk crystals consist of ABC-stacked monolayer assemblies that are held together by van der Waals forces. Thus, the bilayer and trilayer structures are AB and ABC stacking, respectively. In the electronic band structure without spin polarization, all four modalities have an indirect bandgap, as shown in Figure 1b e. In the few-layer form (monolayer, bilayer, and trilayer), the valence band maximum (VBM) is around point and the conduction band minimum (CBM) is at K point. As the number of layers increases, the bandgap narrows down from 2.05 eV (monolayer) to 1.78 eV (trilayer). For the bulk structure, the indirect bandgap of 1.73 eV is the energy dif erence between

VBM along B-Z line and CBM around B point. In addition, note that we use the in-plane lattice constant (6.17 Å) from the experimental data and do not consider spin–orbit coupling and the Hubbard U correction, which may lead to that the calculated bandgap (1.73 eV) is larger than the experimental optical bandgap (1.30 eV) of bulk $FePSe_3$.[45] The corresponding cutoff wavelength of $FePSe_3$ lies in the range from 605 to 717 nm based on the calculated bandgap values from 2.05 to 1.73 eV depending on the thickness. However, the particularity of the $FePSe_3$ crystal is that Fe^2 has a nearly octahedrally coordinated structure. The ground state and excited state of the Fe^2 in a crystal field are ${}^5T_{2g}$ orbital triplet and ${}^5E_g$ orbital doublet, respectively. To quantify the energy difference between Fe-d-t_{2g} (low-lying) and e_g (high-lying) states in $FePSe_3$, we estimate the relative on-site energy of each Fe-d orbital with maximally localized Wannier functions (MLWFs) obtained with the Wannier90 package.[46] The Fe-d orbital is adopted as projections to construct WFs. Appropriate inner and outer energy windows are used during the disentanglement procedure. The calculated split value of the t_{2g} and e_g in $FePSe_3$ is 0.70 eV, which is consistent with the experimental room-temperature optical absorption for the ${}^5T_{2g}$ ${}^5E_g$ transitions, i.e., actually is ascribed to the t_{2g} e_g excitations that is a wide band ranging from 1400 nm (0.89 eV) to 1650 nm (0.75 eV).[44] This means the optical absorption of $FePSe_3$ can extend to the NIR-SWIR spectra. A similar IR absorption has been reported on MoS_2 atomic layers taking advantages of the IR absorption of MoS_2 at 6–9 m wavelengths.[47]

The structures, quality, and average stoichiometry of $FePSe_3$ bulk single crystals were characterized by X-ray diffraction (XRD) patterns and energy-dispersive X-ray (EDX) spectroscopy (Figure S1, Supporting Information). The crucial peak of $FePSe_3$ single crystal is the XRD (003) diffraction peak located at 2θ 13.3 . In addition, the XRD pattern of the single crystal is exactly corresponding to the (00l) diffraction peaks of the $FePSe_3$, and no peaks of other impurity phases were observed (Figure S1a, Supporting Information). The EDX spectroscopy shows that the average atomic ratio of $FePSe_3$ single crystal is Fe:P:Se 0.1977:0.2005:0.6019 1:1:3 (Figure S1b, Supporting Information), which is consistent with the expected stoichiometric ratio of the $FePSe_3$ crystals. These results indicate that no significant vacancies were observed in $FePSe_3$ crystals as well as no traces of impurity were detected on the cleaved surfaces. **Figure 2**a shows the schematic of a multilayer-$FePSe_3$ bolometer device consisting of a $FePSe_3$ flake with two Cr/Au electrodes. The naturally suspended atomic layer structure of the $FePSe_3$ is illustrated schematically, which is desirable for bolometer applications. The thicknesses of the $FePSe_3$ flakes were measured using atomic force microscopy (AFM). Specifically, the thickness of a single-layer (1 L) $FePSe_3$ is 0.80 nm, which is consistent with literature.[45] The AFM images and line scans taken on six $FePSe_3$ flakes with thicknesses of 5.04 nm (6 L), 7.85 nm (10 L), 13.73 nm (17 L), 25.72 nm (32 L), 43.87 nm (55 L), and 59.12 nm (74 L) are illustrated in Figure S2a–f and their insets, respectively (Supporting Information). The Raman spectra of these $FePSe_3$ flakes are exhibited in Figure 2b (43.87 nm in thickness) and Figure S4 (Supporting Information) (with flake layer numbers range of 6 74 L) in the Supporting Information. There are five characteristic Raman peaks indexed to the $FePSe_3$ associated with the metal atom vibrations and the P_2Se_6 unit vibrations of D_{3d} symmetry group.[45,48] The highest intensity peak at 210.2 cm^{-1} is associated with the $A_{1g}(\nu_1)$ mode (the symmetric stretching vibration of the P—Se bonds). The other stretching vibration of the P—Se bonds is the $A_{1g}(\nu_2)$ mode at 163.6 cm^{-1}. The peaks at 143.5 and 176.5 cm^{-1} are attributed to the $E_g(\nu_{12})$ and the $E_g(\nu_{11})$ modes, respectively, which do not involve any P—Se bond stretching. The peak at 110.3 cm^{-1} is derived from the metal atom vibrations in the $FePSe_3$ crystals. With decreasing the number of layers of the $FePSe_3$, the Raman signal gradually weakens to the point that it is almost impossible to distinguish the signal from the noise due to the decreased amount of material (9 L) (Figure S4, Supporting Information). On the other hand, the peak at 299.9 cm^{-1} originated from SiO_2 becomes more prominent with decreasing $FePSe_3$ flake thickness due to decreasing signals from thinner $FePSe_3$ and increasing signal from the substrate.

The results from transport R T curves reveal the semiconducting nature of $FePSe_3$ flakes (Figure 2c). The TCR of the 55 L (or 43.87 nm in thickness) $FePSe_3$ flake can be calculated by TCR $(1/R_0) \cdot (dR/dT)$, and the result of TCR as a function of temperature is shown in the inset of Figure 2c. With increasing temperature, the absolute value of the decreases monotonically, which is similar to conventional bolometer materials.[5,49] The TCR value of the 55 L (or 43.87 nm in thickness) $FePSe_3$ flake is as high as 12.89% K^{-1} at low temperature of 123 K, and it can still reach a competitive value of 2.63% K^{-1} at room temperature. To determine the relationship between the room-temperature TCR and the number of layers, we have prepared several samples with different thicknesses (6, 9, 19, 35 and 67 L) and measured their R T curves in the temperature range of 295–353 K. The result is summarized in Figure 2d and Figure S3 (Supporting Information). Specifically, the TCR values obtained are in the range from 2.74 to 2.96% K^{-1} at room temperature. This result, in combination with that on the two previously measured samples (35 and 55 L), indicates that the intrinsic TCR of the $FePSe_3$ around 2.9% K^{-1} is nearly independent of the sample thickness. This is expected from the very weak interlayer interactions in 2D $FePSe_3$ atomic layers. It is worth noting that the TCR value of $FePSe_3$ is slightly larger than that of the commercial VO_x bolometer (typical about 2% K^{-1}).[5] This implies that the ternary $FePSe_3$ atomic layers is a promising candidate material for a bolometer-type uncooled infrared detector. Based on the TCR and bandgap results described above, we can propose the operating principle of the $FePSe_3$ detector under the illumination of different wavelengths (Figure 2e). When the photon energy $h\nu$ is greater than the bandgap of $FePSe_3$, the $FePSe_3$ layers could absorb photons to generate the excitons (photogenerated carriers) through interband E_v E_c transitions, and the excitons can dissociate into free holes and electrons by the applied bias voltage between the two electrodes. Therefore, the device behaves like a photoconductor and the changes the conductivity of the $FePSe_3$ semiconductor channel is regarded as the photoconductive response. It should be noted that lower energy photons beyond the optical cutoff of the $FePSe_3$ can be absorbed via the ${}^5T_{2g}$ ${}^5E_g$ transitions, resulting in the resistance decrease of the $FePSe_3$ channel due to the excitons dissociation to phonons (or lattice vibration) or heat (bolometric effect).

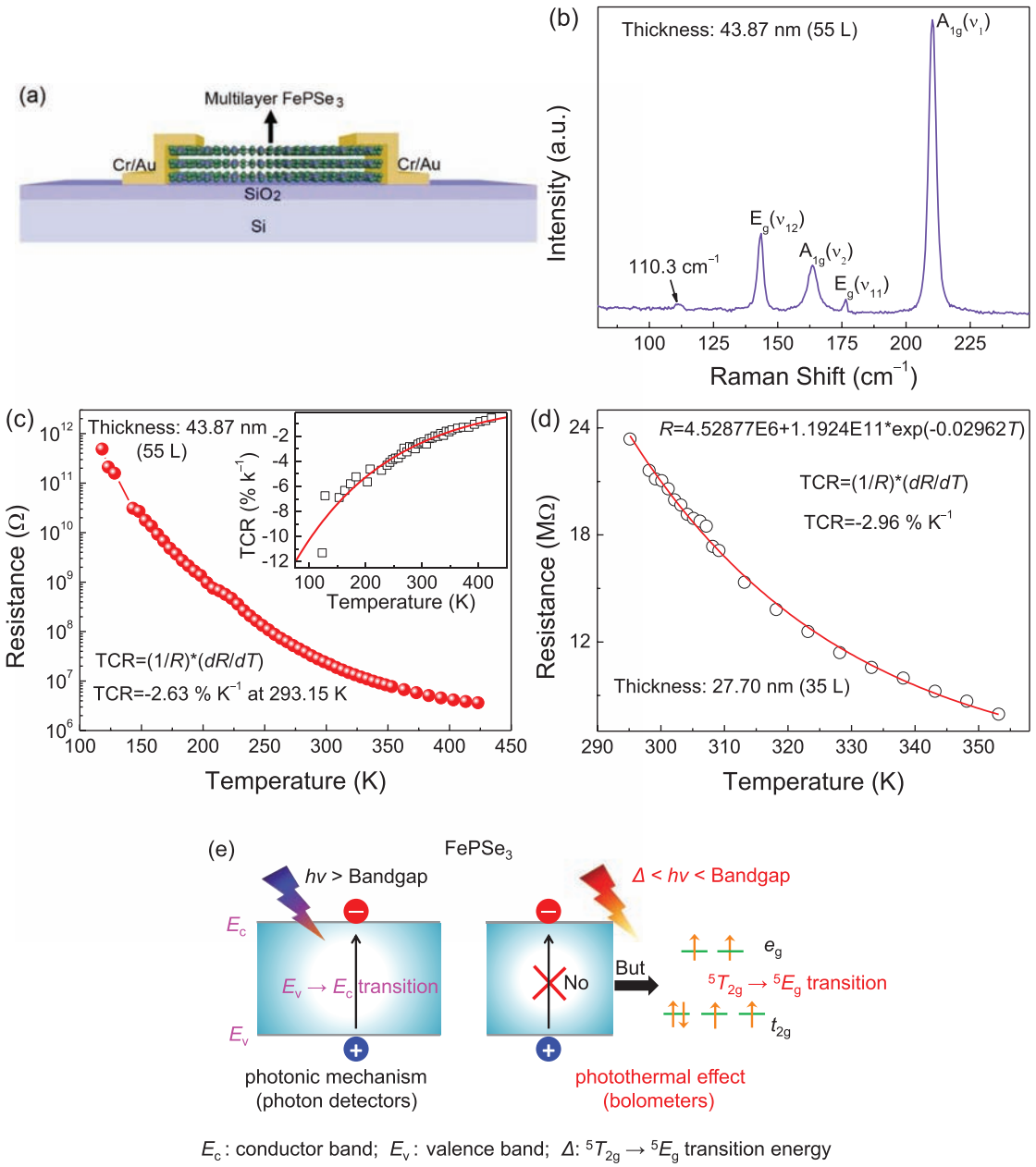

Figure 2. a) Schematic sideview of $FePSe_3$ bolometer device. b) Raman spectrum of the 55-layer $FePSe_3$ f ake. Resistance R versus temperature T of the c) 55-layer $FePSe_3$ f akes and d) 35-layer $FePSe_3$ f ake. Inset shows the extracted TCR of the 55-layer $FePSe_3$ f akes as a function of temperature. e) Schematic diagram of the operating principle of the $FePSe_3$ detector under the illumination of dif erent wavelength bands.

The obtained photoresponse characteristics of the $FePSe_3$ devices with various layer numbers (6 74 L) are illustrated in **Figure 3**a as well as Figure S5 (Supporting Information) at various excitation wavelengths (400 1550 nm) with dif erent optical powers. The linearity in the V_{ds} I_{ds} curves indicates a good ohmic contact between $FePSe_3$ f ake and Ti/Au electrode and is anticipated for a bolometer or photoconductor. The photoinduced voltage (photovoltage, V_{ph}) can be def ned as the dif erence of the voltage in light and the dark, which is linearly dependent on the current (Figure 3b). The device can generate V_{ph} as high as 7 mV even when the incident light power is as low as 0.075 nW, illustrating the benef t of the naturally suspended layered structure of the $FePSe_3$ f akes. Dynamic photoresponse measured on the $FePSe_3$ bolometers are shown in Figure 3c. The rise (and fall) time is def ned as the time from 10% to 90% (from 90% to 10%) of the maximum photovoltage in response to IR illumination of 980 nm (blue), 1064 nm (purple), and 1550 nm (red) wavelengths, respectively. As illustrated in Figure 3d, the rise/fall times of the $FePSe_3$ bolometer are 0.68/0.75 and 0.76/0.91 s under 1064 and 1550 nm excitation, respectively, demonstrating promising performance for practical applications.

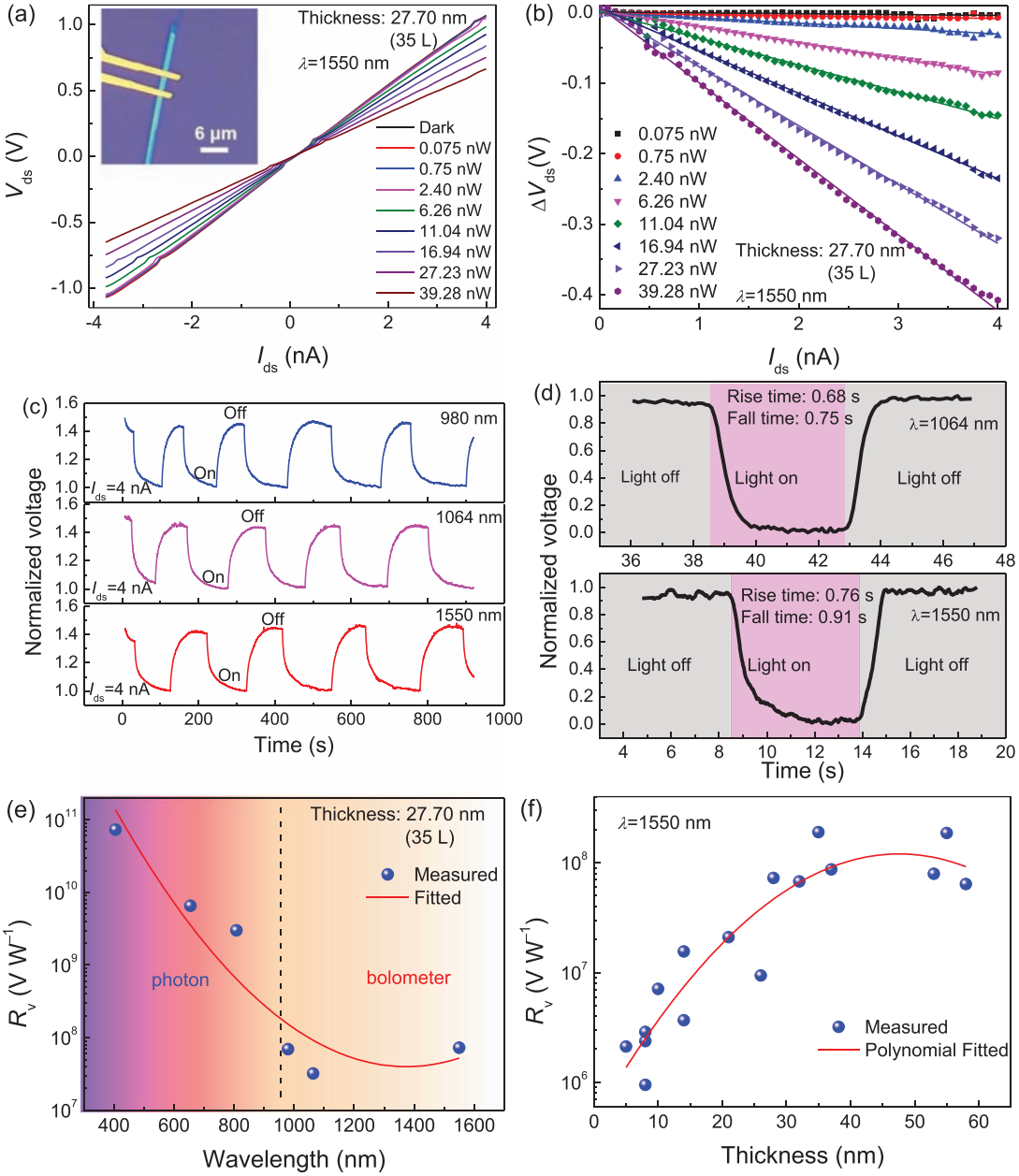

Figure 3. a) V_{ds}–I_{ds} curves of the 35 L $FePSe_3$ bolometer in the dark and under 1550 nm irradiation with various powers. b) Photovoltage (V_{ph}) versus current curves extracted from the V_{ds}–I_{ds} curves in (a). c) Temporal voltage response under various NIR–SWIR wavelengths of 980, 1064, and 1550 nm. d) Response time of the $FePSe_3$ bolometers. e) Responsivity R_v of the 35 L $FePSe_3$ bolometer as a function of wavelength. f) R_v versus thickness of the bolometer under 1550 nm irradiation.

An important f gure of merit used to evaluate the performance of a bolometer is the voltage responsivity R_v, which is the photovoltage V_{ph} divided by the light power P_{in}: R_v V_{ph}/P_{in}, where P_{in} is equal to the product of the incident optical power density P_d and the ef ective detection area S of the device. The R_v of devices with various layer numbers (6 74 L) at various excitation wavelengths (400 1550 nm) have been calculated (Figure 3e and Figure S6, Supporting Information). The R_v of the 35 L-thick $FePSe_3$ bolometer is as high as 10^{10} 10^{11} V W ^{1} when the excitation wavelength is in the ultraviolet–visible spectra. Remarkably, the R_v of the 35 L-thick $FePSe_3$ can reach up to 5 10^{7} V W ^{1} in the NIR band. Obviously, when the energy of the incident photon is larger than the bandgap of $FePSe_3$ (the corresponding cut-of wavelength is 954 nm), the responsivity is signif cantly higher, which is not surprising considering the higher carrier energy and hence mobility. At the illumination of lower energy IR photons (Δ $h\nu$ Bandgap), the absorbed photon energy through the intraband $^5T_{2g}$ ^5E_g transitions is converted primarily to phonons (or lattice vibration) or heat in the $FePSe_3$. The resulting responsivity is typically lower as shown in Figure 3e. This further indicates that there are two main mechanisms for the photoresponse of $FePSe_3$ devices

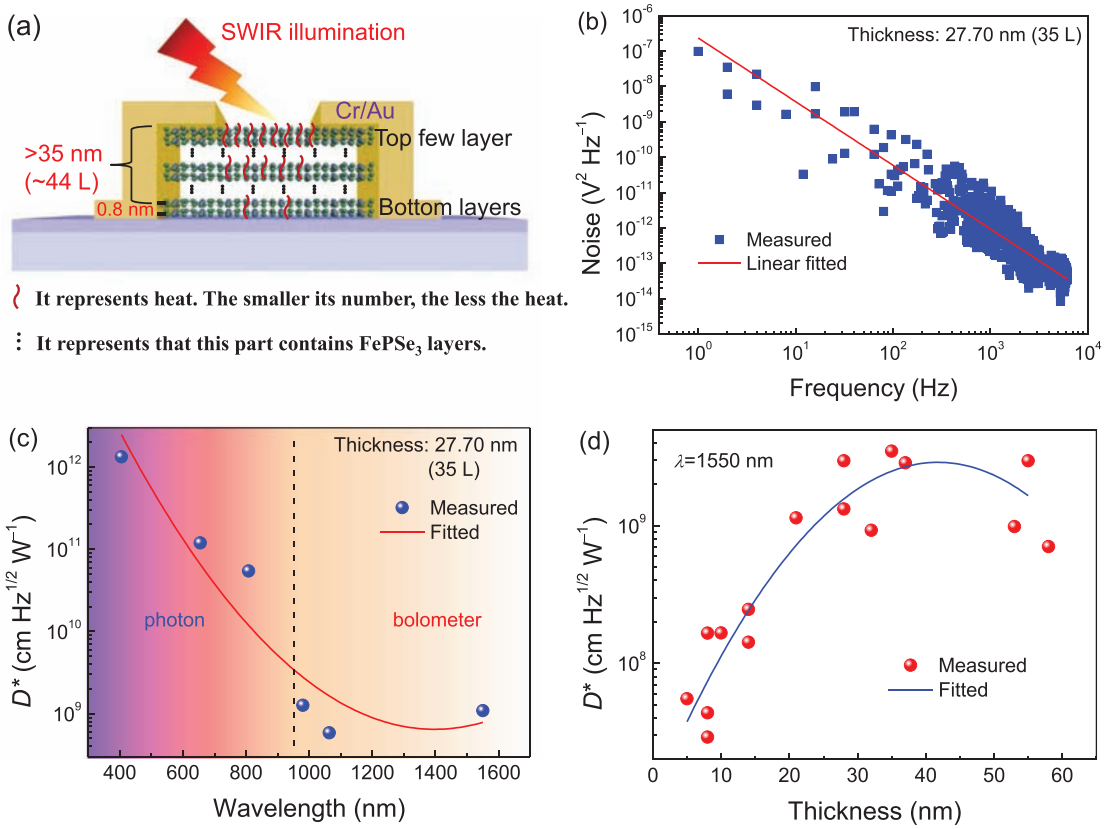

Figure 4. a) Schematic diagram shows the thermal isolated ef ect that the layer number of $FePSe_3$ f ake would af ect the thermal link. b) Spectrum of voltage noise power density (V_n^2) for the 35 L $FePSe_3$ bolometer. A linear fit (solid red line) shows that the 1/*f* noise dominates the noise level of this device. c) Specific detectivity *D** as a function of wavelength for the 35 L $FePSe_3$ bolometer. d) *D** versus thickness under 1550 nm irradiation.

under dif erent incident wavelengths: the photoconductive ef ect at wavelengths above the optical cutof 954 nm and the bolometric ef ect at longer wavelengths beyond the cutof as proposed in Figure 2e.

To better compare the performance of the $FePSe_3$ bolometer, the R_v as a function of the thickness of the $FePSe_3$ under 1550 nm light illumination is shown in Figure 3f. The results show that the R_v value of the $FePSe_3$ bolometer can reach up to 1 10^8 V W ^{1}, which is 2 3 orders of magnitude higher than that of the commercial VO_x bolometer (10^4 10^5 V W ^{1}) in the same spectral range.[5,49] Unlike most commercial bolometers that use a suspended structure to reduce the thermal link between the device and surrounding, no suspended structure was used for the $FePSe_3$ bolometers. Therefore, the high bolometric performance obtained in this work illustrates a distinctive advantage of the $FePSe_3$ 2D atomic layer stacks for bolometer applications. Interestingly, Figure 3f exhibits a strong thickness dependence of the R_v values. When the layer number of the $FePSe_3$ increases from 5 to 35 nm, the R_v value increases monotonically, which may be attributed to increasing benef t of the $FePSe_3$ top layers being thermally isolated, resulting in large ΔT, and hence large ΔR TCR ΔT (proportional to responsivity). At larger thickness above 35 nm (or 44 L), the R_v saturates, followed by a slightly decreasing R_v with further thickness increase. While the specif c mechanism responsible for this trend needs more systematic investigation, a plausible argument is that at a larger thickness beyond 35 nm, the IR photon absorption and therefore heating of the bottom layers in the $FePSe_3$ may not be as efficient as the top layers. As the bottom layers (inactive element) are in parallel to the top layers (active element) of the bolometer, a saturation of the R_v at the critical thickness around 35 nm is anticipated, at which the inactive element is negligible. Reduction of the R_v values would occur when the inactive element provides an alternative electron transfer path in parallel to the active one, as illustrated schematically in **Figure 4**a where a schematic shows the thermal isolated ef ect that the layer number of $FePSe_3$ f ake would af ect the thermal link due to the naturally suspended structure of the 2D van der Waals stacks.

To characterize the noise level of our device, the noise power density (v_n^2) spectrum of the dark voltage of the 35 L (or 27.70 nm in thickness) $FePSe_3$ bolometer was measured and f tted with the 1/*f* noise model (the solid red line), as shown in Figure 4b. The overwhelming 1/*f* noise coming from the random temperature f uctuations is unavoidable in almost all detectors. The noise equivalent power (NEP) is def ned as the signal power when signal-to-noise ratio is unity, given by $NEP = \overline{v_n^2}^{1/2}/R_v = RMS(v_n)/R_v$ in units of W Hz $^{1/2}$, where $RMS(v_n) = \overline{v_n^2}^{1/2}$ is the root-mean-square voltage noise calculated from the spectra of noise power density. Here, the $RMS(v_n)$ value of 35 L (or 27.70 nm in thickness) $FePSe_3$ bolometer is 2.75 10^{10} V Hz $^{1/2}$. The voltage noise spectra of other $FePSe_3$

bolometers with dif erent thicknesses were measured and the RMS(v_n) values were calculated as well (Figure S7, Supporting Information).

Another typical f gure of merit used to evaluate the bolometer performance is the specif c detectivity D^*, def ned as $D^* = S^{1/2}/\mathrm{NEP} = R_v S^{1/2}/\overline{v_n^2}^{1/2}$. We measured the photoresponse of a series of devices with various layer numbers at room temperature and calculated the D^* values under dif erent excitation wavelengths (Figure 4c, Figure S8, Supporting Information). The D^* value is in positive correlation with the wavelength in shorter wavelengths and almost constant in longer wavelengths. The D^* of the 35 L (or 27.70 nm in thickness) $FePSe_3$ bolometer is as high as 10^{11} 10^{12} cm $Hz^{1/2}$ W^{-1} under the illumination wavelengths range from visible to ultraviolet. The D^* as a function of the thickness under 1550 nm light illumination at room temperature is shown in Figure 4d. Similar to the relationship between R_v and thickness, the D^* increases initially as the $FePSe_3$ thickness increases from 5 to 35 nm and reaches a maximum value at 35 nm. Besides, the low noise leads to a potential high detection sensitivity. It is worth noting that the D^* values can reach up to 1 10^9 cm $Hz^{1/2}$ W^{-1} at room temperature. As we have mentioned, the commercial VO_x or other bolometers must use suspended structures to cut the thermal links of the bolometer and its surrounding to obtain high signal-to-noise ratios. The competitive performance demonstrated in the naturally suspended ternary $FePSe_3$ bolometers to the previously reported on the state-of-the-art commercial suspended VO_x bolometer[5,49] suggests $FePSe_3$ and possibly other 2D materials are promising materials for IR bolometer applications at room temperature.

3. Conclusion

In summary, 2D $FePSe_3$ atomic layers with dif erent thicknesses in the range of 5.04 nm (6 L) to 59.12 nm (74 L) have been used for fabricating high-performance uncooled bolometers. High R_v and D^* of 10^{10} 10^{11} V W^{-1} and 10^{11} 10^{12} cm $Hz^{1/2}$ W^{-1}, respectively, have been achieved on the $FePSe_3$ bolometers under the illumination wavelengths ranging from ultraviolet to visible spectra. In NIR SWIR spectra, the uncooled R_v and D^* of the $FePSe_3$ bolometers exhibit an inverted-bell-shaped thickness dependence with the peak R_v and D^* exceeding 1 10^8 V W^{-1} and 1 10^9 cm $Hz^{1/2}$ W^{-1} under 1550 nm SWIR illumination at 35 nm $FePSe_3$ thickness. Remarkably, the performance of the $FePSe_3$ bolometers is on par with the current state-of-the-art conventional bolometers that require suspended structure for thermal isolation and hence improved signal-to-noise ratios. The achieved high bolometer performance can be attributed to: 1) the competitive room-temperature TCR for $FePSe_3$ (2–3)% K^{-1}; 2) the broadband optical absorption extending from UV visible to NIR-SWIR spectra associated to direct interband absorptions at 1.3 eV to lower energy of 0.75 0.89 eV through the $^5T_{2g}$ ^5E_g transitions of Fe^2 in an octahedral ligand f eld; and 3) the unique thermal isolation due to that the $FePSe_3$ atomic layers stacked by the weak van der Waals interlayer force inherit a naturally suspended structure that can ef ectively reduce the device's thermal link to the supporting substrate. Our result demonstrates that the 2D $FePSe_3$ atomic layers can provide a promising candidate material for high-performance uncooled bolometers for miniaturized thermal radiation detection.

4. Experimental Section

Growth, Mechanical Exfoliation, and Transfer of $FePSe_3$ Bulk Single Crystals: $FePSe_3$ bulk single crystals were synthesized using the chemical vapor transport (CVT) method.[45] The high-purity powders of Fe (99.9 %, Alfa Aesar), P (100 mesh, 98.9%, Alfa Aesar), and Se (99 %, Alfa Aesar) at a stoichiometric ratio of 1:1:3 and 10–20 mg I_2 (99.99%, Alfa Aesar) were sealed in a 25-cm-long quartz ampoule at a pressure of less than 10^{-2} Pa. Herein, the I_2 was the transport medium. The quartz ampule was then placed in a two-zone tube furnace. The temperature of the growth and source ends were kept at 600 and 650 C, respectively, for 7 d before the quartz ampule was air-cooled to room temperature. The as-grown crystal structures and quality were characterized by powder XRD using Cu-Kα radiation source (λ 1.5406 Å) (Rigaku SmartLab-9 KW). The average stoichiometric ratio of $FePSe_3$ crystals was examined by EDX spectroscopy (Elite Plus, AMETEK EDAX). The $FePSe_3$ f akes were prepared using a scotch tape standard mechanical exfoliation method from the $FePSe_3$ bulk single crystals onto the polydimethylsiloxane (PDMS). Then, the $FePSe_3$ f akes were transferred to a heavily doped p-type 285 nm-SiO_2/Si substrates by releasing from PDMS. Thus, there are some $FePSe_3$ f akes with dif erent thicknesses on the SiO_2/Si substrates. The $FePSe_3$ samples with dif erent thicknesses were selected according to the optical contrast using the optical microscope (Leica DM4000 M) for subsequent device fabrication, and then their thicknesses are accurately determined by AFM (AFM 5500, Keysight). The quality and the layer numbers of the FePSe3 f akes were characterized using Raman spectroscopy with a 632.8 nm laser (LabRAM HR Evolution).

Calculation on the Electronic Band Structures of $FePSe_3$: The first-principles calculations were performed using the projected augmented-wave method as implemented in the Vienna Ab initio Simulation Package.[50–52] The exchange-correlation functional was modeled by the generalized gradient approximation (GGA) with the Perdew-Burke-Ernzerhof (PBE) realization.[53] The vdW corrections were taken into account by the approach of Dion et al.[54] and the band structures were given by the Heyd-Scuseria-Ernzerhof (HSE06) functional including 25% nonlocal Hartree-Fock exchange.[55] Some tunable parameters were all taken as convergence tests, and the following parameters in each analysis were kept: plane-wave cutof energy, -centered k mesh, and the thickness of the vacuum slab, which were set to 500 eV, 10 10 1 (10 10 10 for the bulk structure), and 20 Å, respectively. To optimize the lattice structures, the energy and force convergence criteria were set to be 10^{-5} eV and 0.01 eV $Å^{-1}$, respectively. And the in-plane lattice constant was set to be 6.17 Å according to the experimental data.

Fabrication and Optoelectronic Measurement of the Devices: The $FePSe_3$ f akes with various thicknesses were transferred to a heavily doped p-type 285 nm-SiO_2/Si substrates preprocessed by acetone, alcohol, and piranha solution (3:1 mixture of sulfuric acid and 30% hydrogen peroxide). The electrodes of the device were made by using standard electron-beam lithography process (FEI-Noval NanoSEM50 with JC Nabity-Nanometer Pattern Generation System), followed by thermal evaporation (DE400EVP, DE Technology) of a Cr/Au film (5/40 nm thick) and lift-of process. All measurements were taken in the atmosphere at room temperature. The semiconductor parameter analyzer (4200-SCS, Keithley) was used to collect the electronic transport signals. The light sources were the continuous-wave semiconductor lasers with wavelengths of 405, 532, 655, 808, 980, 1064, and 1550 nm. To make sure that incident light was collimated, the optical collimating lenses (k9) were installed to the fiber outputs of the lasers. The entire device was illuminated by the collimated incident beam in the experiments. The power of the incident laser beam was measured using a optical power/energy meter (1936-R, Newport) with UV enhanced silicon detector

(918D-UV-OD3R, Newport) at 405–1064 nm and germanium detector (918D-IR-OD3R, Newport) at 1550 nm. During the measurements, a device was placed inside the sealed metal box with a small hole (diameter of 1–2 mm), allowing the laser to pass through and isolate the device from the room light. The incident light power (P_{in}) on the devices could be calculated by P_{in} P_d S, where P_d is the incident power density calculated as the laser output power divided by the cross-sectional area of the laser beam and S is the actual device area measured under microscope. So the responsivity R_v can be calculated as R_v V_{ph}/P_{in} $V_{ph}/(P_d$ $S)$. The dynamic signal analyzer (SR785, Stanford Research) was used to take the noise spectra of $FePSe_3$ devices. A digital oscilloscope (RTO1024, Rohde and Schwarz) and an optical chopper (SR540, Stanford Research) were used to measure the dynamic photoresponse of device.

Supporting Information

Supporting Information is available from the Wiley Online Library or from the author.

Acknowledgements

This work was supported by the Science, Technology and Innovation Commission of Shenzhen Municipality (Grant No. JCYJ20170817110751776) and the National Natural Science Foundation of China (Grant No. 11874193). L.Z. acknowledges the support from the XPLORER PRIZE. Y.F.G. acknowledges support by the National Natural Science Foundation of China (Grant No. 11904312). R.C. acknowledges the supports from the National Natural Science Foundation of China (Grant No. 11574130) and the Science, Technology and Innovation Commission of Shenzhen Municipality (Grant Nos. KQJSCX20170726145748464 and JCYJ20180305180553701). J.W. acknowledges supports from U.S. National Science Foundation (Contract Nos. NSF-DMR-1508494, NSF-ECCS-1809293, and NSF-DMR-1909292). The authors thank Dr. Xiaoming Ma, a Research Assistant Professor from the Shenzhen Institute of Quantum Science and Engineering at the Southern University of Science and Technology, for her help in XRD measurement and discussion.

Conf ict of Interest

The authors declare no conf ict of interest.

Data Availability Statement

The data that supports the findings of this study are available in the supplementary material of this article.

Keywords

2D materials, $FePSe_3$ bolometers, multinary metal phosphorus trichalcogenides, temperature coef cient of resistance

Received: March 28, 2021
Revised: June 28, 2021
Published online: August 23, 2021

[1] A. Koh, S. R. Gutbrod, J. D. Meyers, C. F. Lu, R. C. Webb, G. C. Shin, Y. H. Li, S. K. Kang, Y. G. Huang, I. R. Efimov, J. A. Rogers, *Adv. Healthcare Mater.* **2016**, 5, 373.
[2] P. L. Richards, C. R. McCreight, *Phys. Today* **2005**, 58, 41.
[3] A. Rogalski, *Acta Phys. Pol., A* **2009**, 116, 389.
[4] A. Rogalski, *Infrared Phys. Technol.* **2002**, 43, 187.
[5] A. Rogalski, *Prog. Quantum Electron.* **2003**, 27, 59.
[6] H. J. Zuo, D. Y. Choi, X. Gai, P. Ma, L. Xu, D. N. Neshev, B. P. Zhang, B. Luther-Davies, *Adv. Opt. Mater.* **2017**, 5, 1700585.
[7] E. S. Kulkarni, S. P. Heussler, A. V. Stier, I. Martin-Fernandez, H. Andersen, C. T. Toh, B. Ozyilmaz, *Adv. Opt. Mater.* **2015**, 3, 34.
[8] M. Kopytko, A. Rogalski, *Prog. Quantum Electron.* **2016**, 47, 1.
[9] K. D. Mynbaev, A. M. Smirnov, N. L. Bazhenov, N. N. Mikhailov, V. G. Remesnik, M. V. Yakushev, *J. Electron. Mater.* **2020**, 49, 4642.
[10] P. Martyniuk, W. Gawron, A. Rogalski, *J. Electron. Mater.* **2013**, 42, 3309.
[11] A. Rogalski, P. Martyniuk, M. Kopytko, *Prog. Quantum Electron.* **2019**, 68, 100228.
[12] L. Ciura, A. Kolek, J. Wrobel, W. Gawron, A. Rogalski, *IEEE Trans. Electron Devices* **2015**, 62, 2022.
[13] X. J. Hao, Z. Deng, J. Huang, Y. Huang, H. Yang, Y. Teng, Y. Zhao, Q. H. Wu, X. Li, J. F. Liu, Y. Chen, H. Zhu, B. L. Chen, *IEEE J. Quantum Electron.* **2020**, 56, 4300106.
[14] A. Rogalski, M. Kopytko, P. Martyniuk, *Proc. SPIE* **2017**, 10177, 1017715.
[15] G. Ariyawansa, J. Duran, C. Reyner, J. Scheihing, *Micromachines* **2019**, 10, 806.
[16] E. Gomolka, O. Markowska, M. Kopytko, A. Kowalewski, P. Martyniuk, A. Rogalski, J. Rutkowsk, M. Motyka, S. Krishna, *Bull. Pol. Acad. Sci.: Tech. Sci.* **2018**, 66, 317.
[17] M. Settipalli, S. Neogi, *J. Electron. Mater.* **2020**, 49, 4431.
[18] P. M. Mensz, B. Dror, A. Ajay, C. Bougerol, E. Monroy, M. Orenstein, G. Bahir, *J. Appl. Phys.* **2019**, 125, 174505.
[19] V. S. Krivobok, D. A. Litvinov, S. N. Nikolaev, E. E. Onishchenko, D. A. Pashkeev, M. A. Chernopittsky, L. N. Grigor'eva, *Semiconductors* **2019**, 53, 1608.
[20] A. D. Shen, A. P. Ravikumar, G. P. Chen, K. A. L. Zhao, A. Alfaro-Martinez, T. Garcia, J. de Jesus, M. C. Tamargo, C. Gmachl, *J. Vac. Sci. Technol. B* **2013**, 31, 03C113.
[21] X. F. Wei, W. Y. Wang, J. Fang, R. He, *Physica E* **2020**, 117, 113801.
[22] Y. Kaya, A. Ravikumar, G. P. Chen, M. C. Tamargo, A. D. Shen, C. Gmachl, *AIP Adv.* **2018**, *8*, 075105.
[23] A. Teke, S. Dogan, F. Yun, M. A. Reshchikov, H. Le, X. Q. Liu, H. Morkoc, S. K. Zhang, W. B. Wang, R. R. Alfano, *Solid-State Electron.* **2003**, 47, 1401.
[24] Z. Yang, L. J. Guo, B. Y. Zu, Y. A. Guo, T. Xu, X. C. Dou, *Adv. Opt. Mater.* **2014**, 2, 738.
[25] R. P. Chasmar, W. H. Mitchell, A. Rennie, *J. Opt. Soc. Am.* **1956**, 46, 469.
[26] F. Kohl, F. Keplinger, A. Jachimowicz, J. Schalko, *Sens. Actuator A: Phys.* **2004**, 115, 308.
[27] W. G. Langton, *J. Opt. Soc. Am.* **1946**, 36, 355.
[28] E. S. Awad, N. Al-Khalli, M. Abdel-Rahman, M. Alduraibi, N. Debbar, *IEEE Photonics Technol. Lett.* **2015**, 27, 462.
[29] M. Garcia, R. Ambrosio, A. Torres, A. Kosarev, *J. Non-Cryst. Solids* **2004**, 338, 744.
[30] A. Orduna-Diaz, M. Rojas-Lopez, R. Delgado-Macuil, A. Torres-Jacome, F. J. De la Hidalga-W, D. Ferrusca, S. Ventura-Gonzalez, C. G. Trevino-Palacios, *Proc. SPIE* **2011**, 8011, 80111v.
[31] L. N. Son, T. Tachiki, T. Uchida, *Jpn. J. Appl. Phys.* **2011**, 50, 025803.
[32] Y. Y. Su, X. W. Cheng, J. B. Li, Y. K. Dou, F. Rehman, D. Z. Su, H. B. Jin, *Appl. Surf. Sci.* **2015**, 357, 887.
[33] H. Li, G. Dong, K. Chu, X. Pu, Z. Li, H. Zhang, Q. Chen, X. Liu, *J. Mater. Chem. C* **2020**, *8*, 17054.
[34] H. Li, K. Chu, X. Pu, S. Zhang, G. Dong, Y. Liu, X. Liu, *J. Alloys Compd.* **2020**, 847, 156417.
[35] P. W. Kruse, *Uncooled Thermal Imaging: Arrays, Systems, and Applications*, SPIE, Bellingham, WA **2001**.
[36] A. Rogalski, *Infrared Detectors*, CRC Press, Boca Raton, FL **2010**.

[37] A. Rogalski, M. Kopytko, P. Martyniuk, *Opto-Electron. Rev.* **2020**, *28*, 107.
[38] A. Rogalski, M. Kopytko, P. Martyniuk, *Appl. Phys. Rev.* **2019**, 6, 021316.
[39] R. Gusmeao, Z. Sofer, M. Pumera, *Adv. Funct. Mater.* **2019**, 29, 1805975.
[40] T. A. Shifa, F. M. Wang, Z. Z. Cheng, P. He, Y. Liu, C. Jiang, Z. X. Wang, J. He, *Adv. Funct. Mater.* **2018**, *28*, 1800548.
[41] T. Gao, Q. Zhang, L. Li, X. Zhou, L. G. Li, H. Q. Li, T. Y. Zhai, *Adv. Opt. Mater.* **2018**, 6, 1800058.
[42] C. C. Mayorga-Martinez, Z. Sofer, D. Sedmidubsky, S. Huber, A. Y. S. Eng, M. Pumera, *ACS Appl. Mater. Interfaces* **2017**, 9, 12563.
[43] R. Brec, D. M. Schleich, G. Ouvrard, A. Louisy, J. Rouxel, *Inorg. Chem.* **1979**, *18*, 1814.
[44] E. Banda, *Phys. Status Solidi B* **1986**, *138*, K125.
[45] K. Z. Du, X. Z. Wang, Y. Liu, P. Hu, M. I. B. Utama, C. K. Gan, Q. H. Xiong, C. Kloc, *ACS Nano* **2016**, 10, 1738.
[46] A. A. Mostofi, J. R. Yates, G. Pizzi, Y. S. Lee, I. Souza, D. Vanderbilt, N. Marzari, *Comput. Phys. Commun.* **2014**, *185*, 2309.
[47] A. Goswami, P. Dhandaria, S. Pal, R. McGee, F. Khan, Ž. Antić, R. Gaikwad, K. Prashanthi, T. Thundat, *Nano Res.* **2017**, 10, 3571.
[48] M. Scagliotti, M. Jouanne, M. Balkanski, G. Ouvrard, G. Benedek, *Phys. Rev. B* **1987**, 35, 7097.
[49] C. H. Chen, X. J. Yi, X. R. Zhao, B. F. Xiong, *Sens. Actuator A: Phys* **2001**, 90, 212.
[50] P. E. Blochl, *Phys. Rev. B* **1994**, 50, 17953.
[51] G. Kresse, J. Furthmuller, *Phys. Rev. B* **1996**, 54, 11169.
[52] G. Kresse, J. Hafner, *Phys. Rev. B* **1994**, 49, 14251.
[53] J. P. Perdew, K. Burke, M. Ernzerhof, *Phys. Rev. Lett.* **1996**, 77, 3865.
[54] M. Dion, H. Rydberg, E. Schroder, D. C. Langreth, B. I. Lundqvist, *Phys. Rev. Lett.* **2004**, 92, 246401.
[55] J. Heyd, G. E. Scuseria, M. Ernzerhof, *J. Chem. Phys.* **2003**, *118*, 8207.